Int. J. Electrochem. Sci., 16 **(2021)** Article Number: 211025, doi: 10.20964/2021.10.30

International Journal of
ELECTROCHEMICAL
SCIENCE
www.electrochemsci.org

Short Communication

Steady-state Simulation Analysis of Proton Exchange Membrane Fuel Cell for UAV

Jing Yu, Rongqiang Guan[*], *Mingyue Li, Zichao Liu, Jingjing Yan*

Jilin Engineering Normal University, Changchun, Jilin, 130052, P.R. China
[*]E-mail: rongqiangguan9@sina.com

Received: 15 June 2021 / *Accepted:* 6 August 2021 / *Published:* 10 September 2021

Proton exchange membrane fuel cell (PEMFC) is the most promising power unit in UAV. There are a number of factors that affect the performance of PEMFC, such as operating pressure, operating temperature and relative humidity. In this work, models were adopted to explore the effects of parameters such as operating pressure, operating temperature, and diffusion layer thickness on the steady-state performance of the PEMFC. The results demonstrate that increasing the cathode and anode working pressure is beneficial to the overall performance of the battery. The cathode working pressure has a significant effect on improving the cell efficiency when the cell is operated at a high current density. The increase in operating temperature results in the decrease of the hydrogen partial pressure and oxygen partial pressure, with the effect on the hydrogen partial pressure being more significant. The cell temperature increases in a certain range of operating temperature, while the thermodynamic potential, ohmic polarization potential and activation polarization potential all decrease.

Keywords: Proton exchange membrane fuel cell; Hydrogen-oxygen partial pressure; Steady-state model; Simulation analysis; Current density

1. INTRODUCTION

An unmanned aerial vehicle (UAV) is an aircraft that can be controlled and reused to perform multiple missions. It consists of an unmanned airframe, propulsion system, flight control, mission equipment, and recovery devices [1–3]. From the research on UAV, it was found that the battery is more prone to problems than other important components. Once a power supply problem occurs, the consequences are often serious and can even affect the safety of the entire UAV [4–6]. The power management system is to manage the fuel cell effectively, being able to monitor the fuel cell stack and each individual cell in real time [7,8]. Meanwhile, it needs to realize the online estimation of remaining power and the safety protection function to improve the overall performance of the fuel cell [9,10].

With the development of technology, several types of fuel cells have been developed. A common way of classification is based on the operating temperature and electrolyte [11,12]. According to the

electrolyte used for fuel cell operation, there are five types, namely alkaline fuel cell (AFC), proton exchange membrane fuel cell (PEMFC), phosphoric acid type fuel cell (PAFC), molten carbonate fuel cell (MCFC), and solid oxide fuel cell (SOFC) [13–16]. Among them, the PEMFC converts the chemical energy stored in the fuel and the oxidizer directly into electrical energy [17–19]. The fuel of the PEMFC is hydrogen and the oxidizer is oxygen. The reaction process is that the oxidizer reacts with the fuel through the electrode to produce electrical energy. The catalytic oxidation reaction occurs at the anode and the catalytic reduction reaction occurs at the cathode of a proton exchange membrane fuel cell [20–37].

With the continuous development of computer technology, computer simulation plays an increasingly important role in scientific research. In the study of PEMFC, an accurate and effective mathematical model can clearly describe various fundamental phenomena in fuel cells [38]. In addition, it can also predict the performance of the cells under different structural and operating conditions to optimize the design of the cell system. In order to better understand and thus optimize the fuel cell system, a number of researchers have performed modeling and computer simulations of H_2/O_2 PEM fuel cells. Through different stages of development, the models have gradually developed from simple one-dimensional half-cell mathematical models to complex three-dimensional full-cell mathematical models. Moreover, the development of CFD technology has promoted an increasing application of CFD in the modeling of PEMCF [39,40]. Currently, the purpose of numerical simulation mainly focuses on the development of mathematical models that can be used to analyze the effects of specific battery design and battery material parameters on battery performance. In this work, a steady-state model of a proton exchange membrane fuel cell was developed based on heat transfer, mass transfer, and electrochemistry in an environmental interface. The model was compared with experimental results. With the established steady-state model, the effects of cell reaction gas pressure, cell temperature, and relative humidity on cell characteristics were examined. The effect of reaction conditions on various cell potentials and cell efficiencies was further investigated through simulations.

2. EXPERIMENTAL

2.1. Battery parameters

The experimental single cells were designed and assembled by Jilin Engineering Normal University. The cell air flow channel is a serpentine flow channel. The main cell parameters are shown in Table 1.

Table 1. Battery parameters.

Parameter	Value
Catalyst platinum loading (mg/cm^2)	0.3
Cell reaction area (cm^2)	40
Film thickness (μm)	41
Cathode and anode diffusion layer (mm)	0.5
Size	12×6×3

2.2. Test Systems

The experiments were conducted with an ElectroChem test system being the main test equipment, which is capable of displaying control parameters and test results in real time. The system includes a working pressure test, a reaction gas flow test and a reaction excess factor test. The cathode is supplied with air (20% oxygen, 80% nitrogen). The anode is supplied with hydrogen gas. The test conditions are shown in Table 2.

Table 2. Test conditions.

Parameters	Value
Temperature (K)	338
Anode pressure (kPa)	200
Cathode pressure (kPa)	220

2.3. Activated polarization potential

The polarization potentials for anode and cathode activation are as follows.

$$V_{act} = -[\xi_1 + \xi_2 \cdot T + \xi_3 \cdot T \cdot ln(C_{O_2}) + \xi_4 \cdot T \cdot ln(I)]$$

$$\xi_1 = -\frac{\Delta G_{ec}}{2F} - \frac{\Delta G_e}{\alpha_c nF}$$

$$\xi_2 = \frac{R}{a_c nF} ln\left[nFAk_c^0 (C_H)^{(1-a_c)} (C_{H_2O})^{a_c}\right] + \frac{R}{2F} ln[4FAk_\alpha C_{H_2}]$$

$$\xi_3 = \frac{R(1-\alpha_c)}{\alpha_c nF}$$

$$\xi_4 = -(\frac{R}{2F} + \frac{R}{\alpha_c nF})$$

Where ΔG_{ec} is free energy of chemisorption activation in the standard state. F is Faraday constant (96487 C/mol). A is the effective active area of the battery. k_a^0 is the intrinsic rate constant of the anode reaction. k_c^0 is the intrinsic rate constant of the cathode reaction. R is the gas constant.

Based on the report published by Mann et al. [41] $\xi_1 = -0.948$

$$\xi_2 = 0.00286 + 0.0002lnA + (4.3 \times 10^{-5}) lnC_{H_2}^*$$

$$\xi_3 = 7.6 \times 10^{-5}$$

$$\xi_4 = -1.92 \times 10^{-4}$$

For the currently used PEMCF, this paper adopts the Fmincon function in the Matlab optimization toolbox to optimize the parameters of $R_c, B, I_{max}, \xi_1, \xi_2, \xi_3, \xi_4$. To optimize this function, we need to understand the range of optimization parameters, and set the following parameter ranges:

$$R_c = 0.001$$

$$B = 0.5$$

$$I_{max} = 1250$$

2.4. Battery efficiency calculation

The calculation of the battery efficiency can be expressed by the following equation:

$$\eta = \mu_f \frac{V_{FC} \cdot i}{E_{Nernst} \cdot i}$$

Where μ_f is fuel utilization, which indicates the ratio of the mass of fuel reacting in the cell to the mass of fuel entering the battery. The estimated value used in this paper is 0.95. V_{FC}, i and E_{Nernst} are refer to cattery output voltage, operating current and thermodynamic potential, respectively.

3. RESULTS AND DISCUSSION

Figure 1A-D shows the effect of anode pressure on the various potentials of the cell. It can be seen that the anode pressure has no effect on the ohmic polarization potential, activation polarization potential, or concentration difference polarization potential. The thermodynamic potential increases with the anode side pressure [42], but the increase is small. Therefore, the variation of the anode side pressure has little effect on the performance of the cell.

Figure 1E-H shows the effect of cathode pressure on various potentials of the cell. It can be found that when the cathode pressure increases from 50 kPa to 220 kPa, the ohmic polarization potential and the concentration polarization potential do not change, while only the thermodynamic potential and the activation polarization overpotential change. The cell thermodynamic potential only increases by nearly 0.02 V, while the activation polarization overpotential of the cell decreases by nearly 0.06 V. Therefore, increasing the pressure on the cathode can reduce the loss of activation polarization potential, thus improving the cell performance.

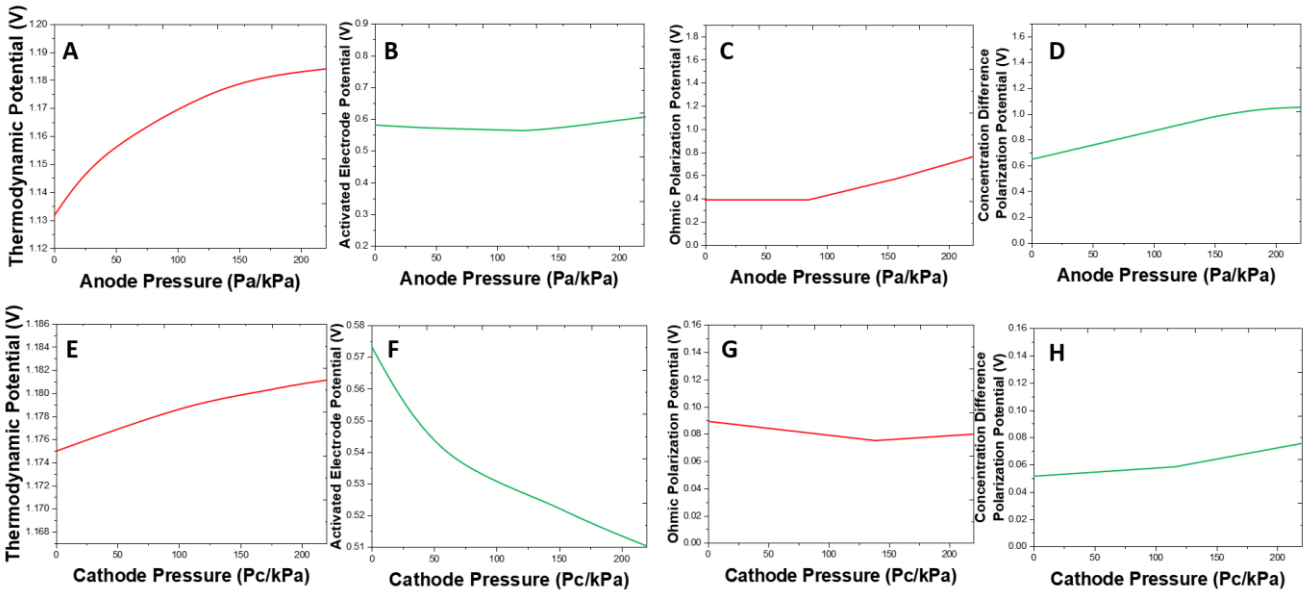

Figure 1. Effect of anode pressure on (A) thermodynamic potential, (B) activated electrode potential, (C) ohmic polarization potential and (D) concentration difference polarization potential. Effect of cathode pressure on (E) thermodynamic potential, (F) activated electrode potential, (G) ohmic polarization potential and (H) concentration difference polarization potential.

Figure 2 shows the effect of temperature on each diffusion coefficient. It can be seen from the figure that each diffusion coefficient increases with the temperature. The diffusion coefficient of hydrogen-oxygen on the anode side is larger than that of the gas on the cathode side [43]. It increases from 295K to about 360K in the temperature range where the cell often works. Water vapor-oxygen and nitrogen-oxygen increase by nearly 50%, and the diffusion coefficient of water vapor-hydrogen becomes 25% larger. Therefore, the increase in temperature has a greater effect on the diffusion of gases on the cathode side than on the anode side [44].

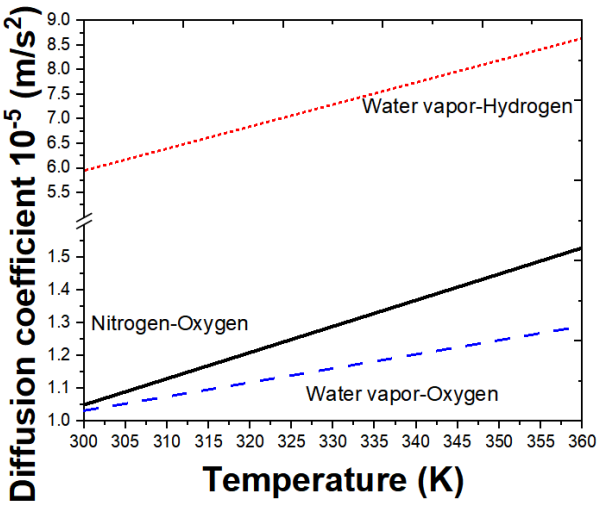

Figure 2. Effect of temperature on hydrogen-oxygen, water vapor-oxygen and nitrogen-oxygen diffusion.

Figure 3A shows the variation of hydrogen and oxygen partial pressures with the cell operating temperature. It can be seen that as the temperature increases, both hydrogen and oxygen partial pressures decrease gradually [45]. With the same range of temperature change, the hydrogen partial pressure varies more than the oxygen partial pressure. Therefore, the difference between the hydrogen and oxygen partial pressures gradually becomes smaller as the battery temperature increases [46]. At temperatures above 340 K, the hydrogen-oxygen partial pressure decreases more rapidly as the cell temperature continues to rise.

Figure 3B shows the variation of the battery voltage with the battery operating temperature being under a stable current operating condition. From the figure, it can be noted that the battery voltage increases as the operating temperature rises [47]. However, when the temperature exceeds 350K, the battery voltage drops rapidly, indicating that the battery can achieve the best results at this operating temperature. The above investigations reveal that the effective partial pressure of the reactive gas in the cell drops relatively lower when the cell operating temperature exceeds 350K, which indicates that the temperature affects the pressure of the reactive gas, leading to the change of the battery efficiency.

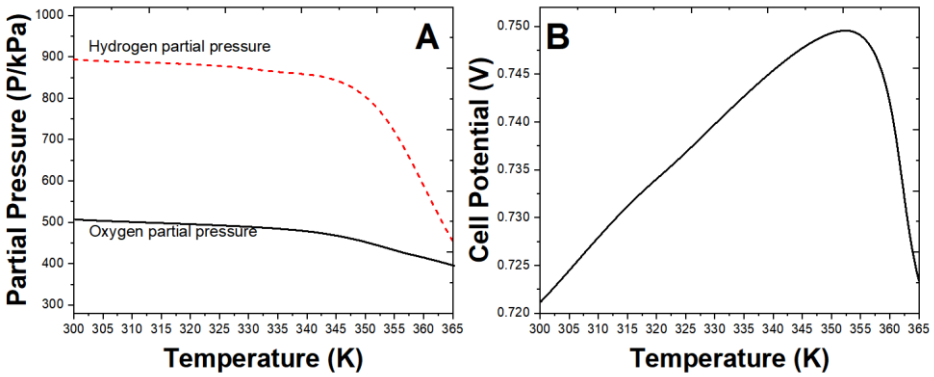

Figure 3. (A) Effect of cell operating temperature on the partial pressure of hydrogen and oxygen. (B) Variation of a battery voltage with battery operating temperature.

The polymer electrolyte must contain enough water, for the reason that the proton conduction capacity of the electrolyte is directly proportional to the water content. However, an excessively high moisture content will cause electrolyte flooding and lead to water blockage of the orifices in its connected electrode or gas diffusion layer [48,49]. Despite that the product of PEMFC is water when it works, the drying effect of air on the electrode at a higher temperature usually exceeds the rate of reaction to produce water. The most common solution to this problem is to humidify the reaction gas before it enters the cell. In this study, we assume that the membrane is at optimal water saturation and we only study the effect of the actual relative humidity inside the cell on the effective partial pressure of hydrogen and oxygen [50–52]. Figure 4A shows the effect of relative humidity on the partial pressures of hydrogen and oxygen, which presents that an increase in relative humidity has a large effect on the effective pressure of both hydrogen and oxygen. As the relative humidity increases from 50% to 100%, the effective partial pressure of hydrogen decreases by nearly 100 kPa, and the effective partial pressure of oxygen decreases by nearly 35 kPa. Therefore, excessive humidification is not good for improving the battery efficiency. In actual battery operation, when excessive humidification is applied, the battery is prone to form water droplets, resulting in flooding and deterioration of battery efficiency.

The PEMCF gas diffusion layer consists of a conductive porous material that supports the catalytic layer, collects the current, conducts the gas and discharges the water, which realizes the redistribution of reaction gas and product water between the flow field and the catalytic layer, and is one of the key components affecting the performance of the electrode.

Figure 4B shows the pressure variation of hydrogen gas along the diffusion direction for different current density operation of the cell. It can be noted from the figure that the effective partial pressure of hydrogen gas follows an almost linear trend with the diffusion distance. As the diffusion distance becomes larger, the effective hydrogen pressure gradually decreases, while the overall pressure decrease is not large. The effective partial pressure of hydrogen decreases faster as the working current density of the cell becomes higher, the main reason for which is the increase in the amount of consumed hydrogen as the operating current density becomes higher.

Figure 4C shows the pressure variation of oxygen along the diffusion direction for different current density operation of the cell. The figure presents that the effective partial pressure of oxygen

follows a nearly linear trend with the diffusion distance, which is similar to that of the anode side. As the diffusion distance becomes larger, the effective pressure of oxygen gradually decreases. In addition, the effective partial pressure of oxygen decreases faster as the working current density of the cell becomes higher, the main reason for which is the increase in the amount of oxygen consumption due to the higher operating current density.

Figure 5 shows the changes of battery efficiency and battery power. As the working current density of the battery increases, the efficiency of the battery tends to decrease, and when the power of the battery reaches the maximum, the efficiency of the battery decreases by about 30%. When the working current density increases, various irreversible voltage losses become larger, which generally shows a decreasing trend in the battery efficiency. When the power reaches the maximum, the performance of the battery is mainly affected by the reactant mass transfer and the efficiency decreases rapidly.

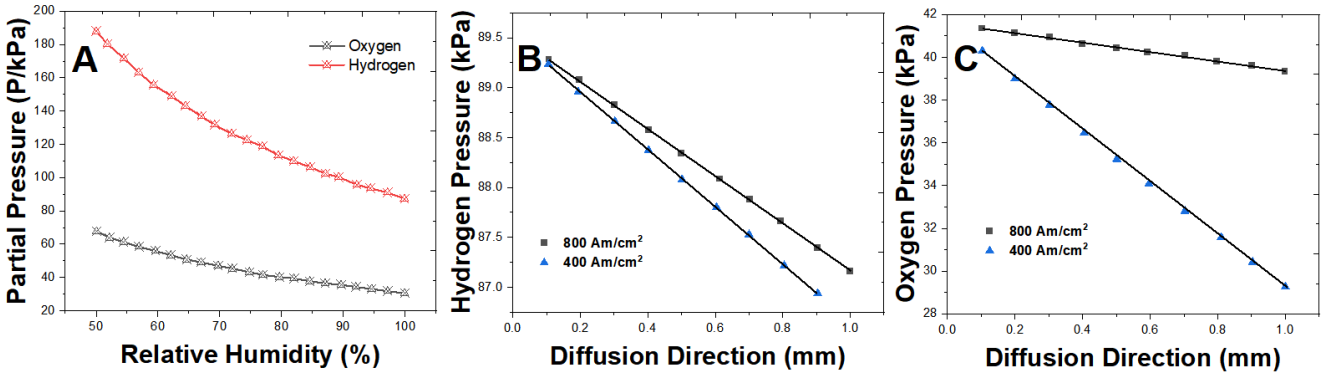

Figure 4. (A) Effect of relative humidity on the partial pressure of hydrogen and oxygen. (B)Pressure distribution in the direction of hydrogen diffusion. (C) Pressure distribution in the direction of oxygen diffusion.

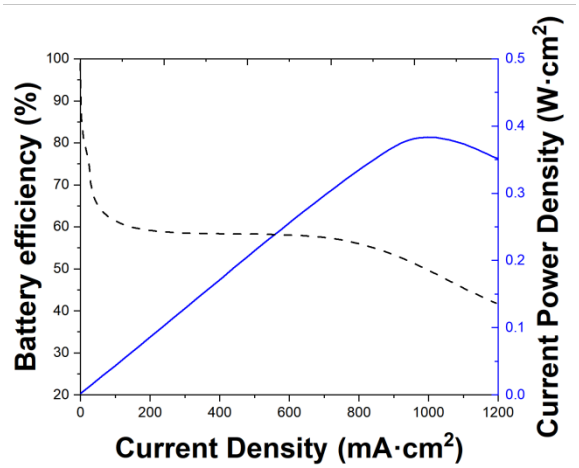

Figure 5. Variation of cell efficiency and cell power density with current density.

Figure 6A compares the effect of cathode pressure on cell efficiency at different current densities, which reveals that the increase in cathode pressure leads to an increase in cell efficiency at different operating current densities. Figure 6B compares the effect of anode pressure on cell efficiency at different current densities, which reveals that the increase in anode pressure leads to an increase in cell efficiency at different operating current densities. However, the overall change in efficiency is not significant, and the effect of increasing anode pressure on the improvement of cell efficiency is not obvious.

Increasing the reactant gas working pressure facilitates the increase of H_2 and O_2 partial pressure, which increases the thermodynamic potential. Particularly, increasing the cathode side pressure can facilitate the decrease of activation polarization potential, compared with increasing the anode pressure [53,54]. The cell is more affected by the mass transfer of reactants at high operating current density, thus the reaction gas pressure increase has a more obvious effect on the cell efficiency promotion [55–58].

Figure 6C shows the effect of cell temperature on cell efficiency at different current densities. As the cell temperature rises from 278K to 368K, the cell efficiency increases more significantly in all cases. When the temperature approaches 360K, the cell efficiency reaches the maximum of high current density. Thereafter, there is a slight decline indicating that the effect of increasing the temperature on the battery efficiency is gradually weakened. In the case that the temperature continues to increase, the battery efficiency will decrease.

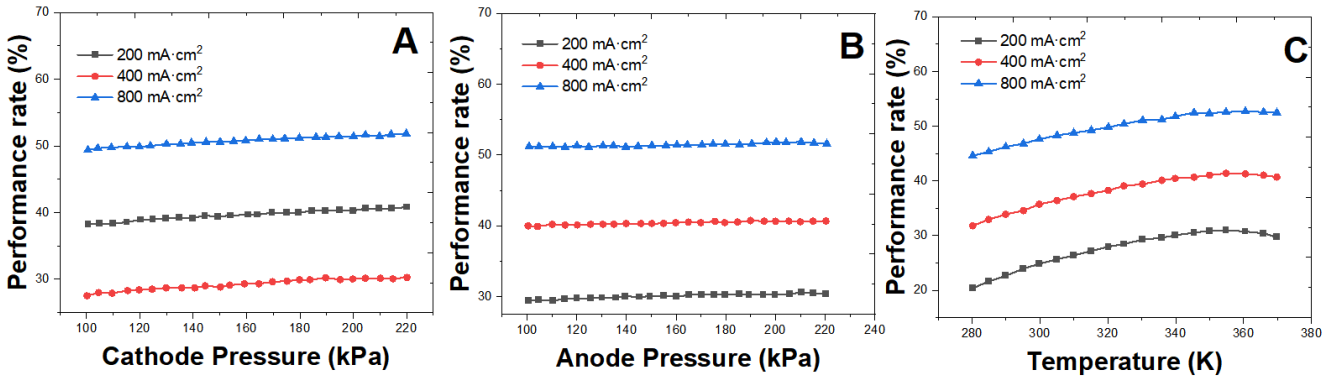

Figure 6. Effect of (A) cathode, (B) anode pressure and (C) temperature on cell efficiency.

4. CONCLUSION

In this study, a steady-state model of PEMCF was developed to simulate the effects of cell operating pressure, operating temperature, and diffusion layer thickness on battery efficiency. Increasing the operating pressure of both cathodes and anodes can improve cell performance and cell efficiency. However, increasing the cathode pressure is more beneficial to the cell performance compare with the increase of the anode pressure, especially in the high current density operation region. Increasing the operating temperature of the battery within a certain range is conducive to reducing the activation

polarization potential and enhancing the battery efficiency. The higher the operating current density is, the more obvious the increase in battery efficiency is. Increasing the cathode and anode pressure with the cell being at a high operating current density can substantially increase the cell efficiency. Nevertheless, as the operating current density becomes higher, the efficiency of the battery gradually decreases.

References

1. T.H. Oh, *Energy Conversion and Management*, 176 (2018) 349–356.
2. B. Wang, D. Zhao, W. Li, Z. Wang, Y. Huang, Y. You, S. Becker, *Progress in Aerospace Sciences*, 116 (2020) 100620.
3. J. Renau, J. Barroso, A. Lozano, A. Nueno, F. Sánchez, J. Martín, F. Barreras, *International Journal of Hydrogen Energy*, 41 (2016) 19702–19712.
4. Ó. González-Espasandín, T.J. Leo, M.A. Raso, E. Navarro, *Renewable Energy*, 130 (2019) 762–773.
5. S. Toghyani, S.A. Atyabi, X. Gao, *Energies*, 14 (2021) 2494.
6. M. Dudek, P. Tomczyk, P. Wygonik, M. Korkosz, P. Bogusz, B. Lis, *Int. J. Electrochem. Sci*, 8 (2013) 8442–8463.
7. Z.U. Bayrak, U. Kaya, E. Oksuztepe, *International Journal of Hydrogen Energy*, 45 (2020) 7036–7045.
8. F. Xie, Z. Shao, M. Hou, H. Yu, W. Song, S. Sun, L. Zhou, B. Yi, *Journal of Energy Chemistry*, 36 (2019) 129–140.
9. M. Dudek, B. Lis, A. Raźniak, M. Krauz, M. Kawalec, *Applied Sciences*, 11 (2021) 675.
10. M. Khzouz, E.I. Gkanas, A. Girella, T. Statheros, C. Milanese, *International Journal of Hydrogen Energy*, 45 (2020) 5384–5394.
11. N. Ramaswamy, S. Mukerjee, *Chemical Reviews*, 119 (2019) 11945–11979.
12. B.G. Pollet, S.S. Kocha, I. Staffell, *Current Opinion in Electrochemistry*, 16 (2019) 90–95.
13. B. Ong, S. Kamarudin, S. Basri, *International Journal of Hydrogen Energy*, 42 (2017) 10142–10157.
14. M.A. Abdelkareem, M.A. Lootah, E.T. Sayed, T. Wilberforce, H. Alawadhi, B.A. Yousef, A. Olabi, *Science of The Total Environment*, 769 (2021) 144243.
15. Y. Wang, D.F.R. Diaz, K.S. Chen, Z. Wang, X.C. Adroher, *Materials Today*, 32 (2020) 178–203.
16. Z. Pan, L. An, C. Wen, *Applied Energy*, 240 (2019) 473–485.
17. G. Zhang, L. Fan, J. Sun, K. Jiao, *International Journal of Heat and Mass Transfer*, 115 (2017) 714–724.
18. S. Bao, A. Ebadi, M. Toughani, J. Dalle, A. Maseleno, A. Yıldızbası, *International Journal of Hydrogen Energy*, 45 (2020) 17882–17892.
19. L. Wang, X. Wan, S. Liu, L. Xu, J. Shui, *Journal of Energy Chemistry*, 39 (2019) 77–87.
20. J. Escorihuela, A. García-Bernabé, Á. Montero, Ó. Sahuquillo, E. Giménez, V. Compañ, *Polymers*, 11 (2019) 732.
21. H. Pourrahmani, M. Moghimi, M. Siavashi, M. Shirbani, *Applied Thermal Engineering*, 150 (2019) 433–444.
22. S. Ratso, N.R. Sahraie, M.T. Sougrati, M. Käärik, M. Kook, R. Saar, P. Paiste, Q. Jia, J. Leis, S. Mukerjee, *Journal of Materials Chemistry A*, 6 (2018) 14663–14674.
23. G. Liu, X. Yang, H. Zhang, L. Fu, *Int. J. Electrochem. Sci*, 15 (2020) 5395–5403.
24. J. Ying, Y. Zheng, H. Zhang, L. Fu, *Revista Mexicana de Ingeniería Química*, 19 (2020) 585–592.

25. M. Zhang, B. Pan, Y. Wang, X. Du, L. Fu, Y. Zheng, F. Chen, W. Wu, Q. Zhou, S. Ding, *ChemistrySelect*, 5 (2020) 5035–5040.
26. W. Long, Y. Xie, H. Shi, J. Ying, J. Yang, Y. Huang, H. Zhang, L. Fu, *Fullerenes, Nanotubes and Carbon Nanostructures*, 26 (2018) 856–862.
27. Y. Zheng, H. Zhang, L. Fu, *Inorganic and Nano-Metal Chemistry*, 48 (2018) 449–453.
28. Y. Zheng, J. Zhu, L. Fu, Q. Liu, *Int. J. Electrochem. Sci*, 15 (2020) 9622–9630.
29. L. Fu, M. Wu, Y. Zheng, P. Zhang, C. Ye, H. Zhang, K. Wang, W. Su, F. Chen, J. Yu, A. Yu, W. Cai, C.-T. Lin, *Sensors and Actuators B: Chemical*, 298 (2019) 126836.
30. Y. Xu, Y. Lu, P. Zhang, Y. Wang, Y. Zheng, L. Fu, H. Zhang, C.-T. Lin, A. Yu, *Bioelectrochemistry*, 133 (2020) 107455.
31. L. Fu, K. Xie, A. Wang, F. Lyu, J. Ge, L. Zhang, H. Zhang, W. Su, Y.-L. Hou, C. Zhou, C. Wang, S. Ruan, *Analytica Chimica Acta*, 1081 (2019) 51–58.
32. Y. Zheng, Y. Huang, H. Shi, L. Fu, *Inorganic and Nano-Metal Chemistry*, 49 (2019) 277–282.
33. H. Karimi-Maleh, B.G. Kumar, S. Rajendran, J. Qin, S. Vadivel, D. Durgalakshmi, F. Gracia, M. Soto-Moscoso, Y. Orooji, F. Karimi, *Journal of Molecular Liquids*, 314 (2020) 113588.
34. H. Karimi-Maleh, A. Ayati, R. Davoodi, B. Tanhaei, F. Karimi, S. Malekmohammadi, Y. Orooji, L. Fu, M. Sillanpää, *Journal of Cleaner Production*, 291 (2021) 125880.
35. H. Karimi-Maleh, Y. Orooji, A. Ayati, S. Qanbari, B. Tanhaei, F. Karimi, M. Alizadeh, J. Rouhi, L. Fu, M. Sillanpää, *Journal of Molecular Liquids* (2020) 115062.
36. H. Karimi-Maleh, M. Alizadeh, Y. Orooji, F. Karimi, M. Baghayeri, J. Rouhi, S. Tajik, H. Beitollahi, S. Agarwal, V.K. Gupta, S. Rajendran, S. Rostamnia, L. Fu, F. Saberi-Movahed, S. Malekmohammadi, *Ind. Eng. Chem. Res.*, 60 (2021) 816–823.
37. H. Karimi-Maleh, Y. Orooji, F. Karimi, M. Alizadeh, M. Baghayeri, J. Rouhi, S. Tajik, H. Beitollahi, S. Agarwal, V.K. Gupta, *Biosensors and Bioelectronics* (2021) 113252.
38. L. Zhang, Z. Ren, Z. Su, Y. Liu, T. Yang, M. Cao, Y. Jiang, Y. Tang, H. Chen, W. Zhang, *The Journal of Clinical Endocrinology & Metabolism*, 106 (2021) 988–998.
39. Y. Peng, H.M. Mahyari, A. Moshfegh, A. Javadzadegan, D. Toghraie, M. Shams, S. Rostami, *International Communications in Heat and Mass Transfer*, 115 (2020) 104638.
40. M. Hosseini, H.H. Afrouzi, H. Arasteh, D. Toghraie, *Energy*, 188 (2019) 116090.
41. R.F. Mann, J.C. Amphlett, M.A. Hooper, H.M. Jensen, B.A. Peppley, P.R. Roberge, *Journal of Power Sources*, 86 (2000) 173–180.
42. S.M. Nosratabadi, R. Hemmati, M. Bornapour, M. Abdollahpour, *Sustainable Energy Technologies and Assessments*, 43 (2021) 100963.
43. M. Sepe, P. Satjaritanun, S. Hirano, I.V. Zenyuk, N. Tippayawong, S. Shimpalee, *Journal of The Electrochemical Society*, 167 (2020) 104516.
44. Y. Lu, R. Steinberger-Wilckens, S. Du, *Electrochimica Acta*, 279 (2018) 99–107.
45. R. Sandström, J. Ekspong, A. Annamalai, T. Sharifi, A. Klechikov, T. Wågberg, *RSC Advances*, 8 (2018) 41566–41574.
46. P. Satjaritanun, S. Shimpalee, J.W. Weidner, S. Hirano, Z. Lu, A. Shum, I.V. Zenyuk, S. Ogawa, S. Litster, *ECS Transactions*, 80 (2017) 187.
47. M. Lindstrom, B. Wetton, *Heat and Mass Transfer*, 53 (2017) 205–212.
48. H. Mehnatkesh, A. Alasty, M. Boroushaki, M.H. Khodsiani, M.R. Hasheminasab, M.J. Kermani, *IEEE Sensors Journal*, 20 (2020) 10679–10686.
49. C. Yan, J. Chen, H. Liu, H. Lu, *IEEE Transactions on Industrial Electronics*, 67 (2019) 2875–2884.
50. N. Dyantyi, A. Parsons, C. Sita, S. Pasupathi, *Open Engineering*, 7 (2017) 287–302.
51. Y. Jiapei, M. Xiao, L. Timan, *Journal of Tsinghua University (Science and Technology)*, 59 (2019) 580–586.
52. J. Liu, Q. Li, H. Yang, Y. Han, S. Jiang, W. Chen, *IEEE Access*, 7 (2019) 92009–92019.
53. H. Chen, X. Zhao, B. Qu, T. Zhang, P. Pei, *Energy Procedia*, 158 (2019) 2290–2298.

54. A. Chitsazan, M. Monajjemi, *French-Ukrainian Journal of Chemistry*, 8 (2020) 95–107.
55. I. Farid, A. Boruah, J. Chutia, A.R. Pal, H. Bailung, *Materials Chemistry and Physics*, 236 (2019) 121796.
56. K. Mohammadzadeh, H. Khaleghi, R. Maddahian, E. Shirani, *Journal of the Brazilian Society of Mechanical Sciences and Engineering*, 42 (2020) 1–13.
57. M. Xu, S. Kang, J. Lu, X. Yan, T. Chen, Z. Wang, *Coatings*, 10 (2020) 183.
58. H. Dong, S. He, X. Wang, C. Zhang, D. Sun, *Diamond and Related Materials*, 110 (2020) 108156.